Assessment of the Climate Variability Effects on Planted Forests (Case study: Dry lands, Semnan Province)

Mohsen Abdolhoseini[1] , Hassan Khosravi[1*] , Ali Tavili[1] ,
Gholamreza Zehtabian[1] , Hamidreza Keshtkar[1] , Esmaeil Heydari Alamdarlou[1]

[1] Department of Reclamation of Arid and Mountainous Regions, Faculty of Natural Resources, University of Tehran, Karaj, Iran. E-mail: hakhosravi@ut.ac.ir

Article Info.	ABSTRACT

Afforestation of wind erosion hotspots using drought-tolerant species such as *Haloxylon* spp. remains a central strategy in mitigating desertification and stabilizing mobile dunes in Iran's arid regions. Despite these efforts, the long-term sustainability of such ecosystems is becoming increasingly uncertain due to the combined pressures of climate variability and anthropogenic disturbances. This study evaluated the ecological resilience of planted desertland forests in Semnan Province by quantifying the relative contributions of climatic and human influences. A time series of Landsat 8 imagery from 2013 to 2022 was used to derive the Forest Canopy Density (FCD) model. Vegetation dynamics were statistically correlated with drought patterns, as measured by the Standardized Precipitation–Evapotranspiration Index (SPEI), using Pearson correlation analysis. The findings revealed that the FCD maintained a consistent range between 44.9% and 55.8%, indicating a moderate and stable vegetation cover characteristic of established Haloxylon stands in arid environments. The correlation analysis revealed a weak and statistically non-significant association ($R = 0.21$, $p > 0.05$, $n = 10$) between FCD and SPEI at a 9-month lag. This lack of significant climatic coupling highlights that precipitation variability alone explains a negligible portion of vegetation dynamics, strongly pointing to the dominance of non-climatic drivers such as anthropogenic disturbances and groundwater dependency. Furthermore, based on the Residual Trend Analysis (RESTREND), the Mann-Kendall trend test on residuals revealed no statistically significant anthropogenic degradation or restoration trends across the study area (Z-values ranging from -1.40 to +1.40). This indicates that human pressures likely remained constant rather than intensified during the 2013–2022 period, resulting in a fragile status quo. The compounded effects of prolonged droughts and unsustainable water resources management thus shape the sustainability of these afforested systems. The adoption of integrated, climate-informed, and human-responsive land management approaches is strongly recommended to safeguard these critical desert ecosystems.

1. Introduction

Historical and cultural records indicate that communities across the Iranian Plateau have long adapted to arid environments through locally developed, sustainable practices, maintaining a delicate balance between limited resource use and environmental preservation (Jiang & Arnold, 2023). However, over the past century, this balance has been profoundly disrupted by population growth, socio-economic transformation, and the intensification of climate change (Barati *et al*., 2023; Rosińska *et al*., 2024; Kompas *et al*., 2024), accelerating the process of desertification—one of the most visible manifestations of global environmental degradation (Ziadat *et al*., 2025). Desertification, a multifaceted phenomenon affecting arid, semi-arid, and dry sub-humid regions, leads to declining soil fertility, biodiversity loss, and far-reaching socio-economic consequences (Jain *et al*., 2024). In response to this challenge, afforestation has been widely promoted as a key intervention to restore degraded landscapes and control desertification processes (Chen *et al*., 2023).

Positioned within the global dry belt, Iran is particularly vulnerable to land degradation. Wind erosion, one of the most damaging forms of land degradation, impacts over 29.5 million hectares nationwide, with approximately 13.9 million hectares designated as wind erosion hotspots (WEHS), where farmlands, infrastructure, and settlements are at risk (Yin *et al*., 2024). To mitigate land degradation, Iran has implemented various desert afforestation programs, particularly focusing on native species such as Haloxylon spp. in critical wind-erosion hotspots.. Over the past five decades, this effort has resulted in more than 1.3 million hectares of shelterbelts, primarily established using *Haloxylon* spp. a native, drought-tolerant genus well-suited to harsh environmental conditions, including high salinity, water scarcity, and elevated temperatures (Guo *et al*., 2014). Today, artificially planted *Haloxylon* forests cover over one million hectares and represent a core component of the nation's desert ecosystem management strategy (Stavi *et al*., 2022).

Despite their initial effectiveness, the long-term ecological health of these planted lands is increasingly under pressure. Widespread signs of decline, such as canopy dieback, stand-level desiccation, and vegetation loss, are particularly evident in older plantations (Li *et al*., 2024). These forests face multiple and interacting stressors, including prolonged drought episodes (Alamdarloo *et al*., 2018), declining groundwater levels, pest outbreaks, and persistent anthropogenic pressures such as overgrazing, illegal logging, and land conversion. There is growing evidence that many of these afforested zones are approaching ecological thresholds beyond which recovery may become extremely difficult or even impossible (Eskandari *et al*., 2016).

Accurate, scalable monitoring tools are urgently needed to assess the health and trajectory of these ecosystems (Wu *et al*., 2024). Although field-based methods provide precise data, their application across vast, remote desert areas is cost-prohibitive and logistically challenging. Remote sensing (RS) has emerged as a critical tool for monitoring vast, inaccessible dryland ecosystems, providing scalable indicators to assess vegetation health, productivity, and responses to climate variability (Wu *et al*., 2024). Various RS-based indicators have been employed to decipher the complex interactions between biotic and abiotic factors in these fragile environments.

The Normalized Difference Vegetation Index (NDVI) and Leaf Area Index (LAI) are among the most widely used indices to monitor vegetation dynamics, greening trends, and biomass production in drylands. For instance, Li *et al*. (2024) used NDVI and Net Primary Productivity (NPP) to assess vegetation responses to climate change in China's drylands, highlighting that while greening is observed in some areas, it does not always correspond to ecosystem stability

due to water constraints. Similarly, Zhang *et al*. (2024) employed these indices to track vegetation cover changes in North and South American drylands, correlating them with precipitation anomalies and land use changes.

Beyond structural indices, RS is increasingly used to monitor functional traits and water stress. Zhang *et al*. (2022) emphasized the importance of monitoring Evapotranspiration (ET) and Vapor Pressure Deficit (VPD) using remote sensing to understand tree transpiration and drought-stress responses. They noted that rising VPD and temperature are critical drivers of forest decline in water-limited regions. Furthermore, Ye *et al*. (2024) demonstrated the utility of integrating high-resolution satellite data (e.g., MODIS) with deep learning models to predict agricultural water demand and soil moisture dynamics, which is crucial for managing water resources in arid regions.

However, standard vegetation indices may be limited in sparsely vegetated desert environments by soil background signals. Wu *et al*. (2024) highlighted the development of indices specific to distinct dryland features, such as the Biological Soil Crust Index (BSCI) and Crust Index (CI), to distinguish biological soil crusts from bare soil and vascular plants. Additionally, Zeng *et al*. (2024) discussed the application of remote sensing to detect signals of shrub encroachment and land degradation in the Mediterranean region, emphasizing the need for fine-resolution imagery to capture subtle changes in ecosystem structure.

Despite the ecological importance and strategic value of these forested regions, there remains a significant gap in the literature. To date, no comprehensive study has examined the long-term sustainability of Iran's desert plantations using multi-decadal satellite observations, nor has there been an integrated attempt to quantify the respective roles of climate change and human activity in forest degradation.

This study seeks to address the following key questions over the timeframe of 2013 to 2022: (1) What are the spatial and temporal trends in forest canopy density and health? (2) Using the Residual Trend Analysis (RESTREND) method, to what extent can observed changes be attributed to climate variability versus anthropogenic drivers? (3) Where are the critical hotspots of degradation and the zones exhibiting ecological resilience?

By integrating multi-temporal satellite archives with advanced remote sensing and machine learning techniques, this research provides a robust foundation for evidence-based ecosystem management, targeted conservation planning, and long-term resilience of Iran's afforested desert landscapes.

2. Materials and Methods
This study aimed to evaluate the sustainability of planted desert forests in Semnan Province and to distinguish the relative impacts of climate variability and human activities. The analysis was conducted using satellite imagery and meteorological datasets within a structured methodological framework.

2.1. Study Area
The study was conducted in Semnan Province, located along the southern slopes of the Alborz Mountain Range in north-central Iran. The province spans approximately 98,000 km², positioned between 34° and 37° N latitude and 51° and 58° E longitude. Semnan features substantial climatic and topographic heterogeneity, extending from high-altitude mountainous regions in the north to vast desert plains in the south. The region receives an average annual precipitation of 132–136 mm and has a mean annual temperature of approximately 19.9 °C,

with a mean elevation of 1,067 m above sea level. This variation supports a range of climate types from semi-arid to hyper-arid.

Desert ecosystems dominate approximately 40% of the province's total area, primarily in the central and southern zones. To combat desertification, extensive afforestation efforts have been implemented, resulting in approximately 1,457 hectares of planted forests, mainly composed of Haloxylon spp.A drought-tolerant shrub species integral to Iran's national anti-desertification programs. These afforested zones, delineated in Figure 1, represent the primary focus of the present study (Ravanbakhsh *et al*., 2023; Ataei & Hasheminasab, 2012).
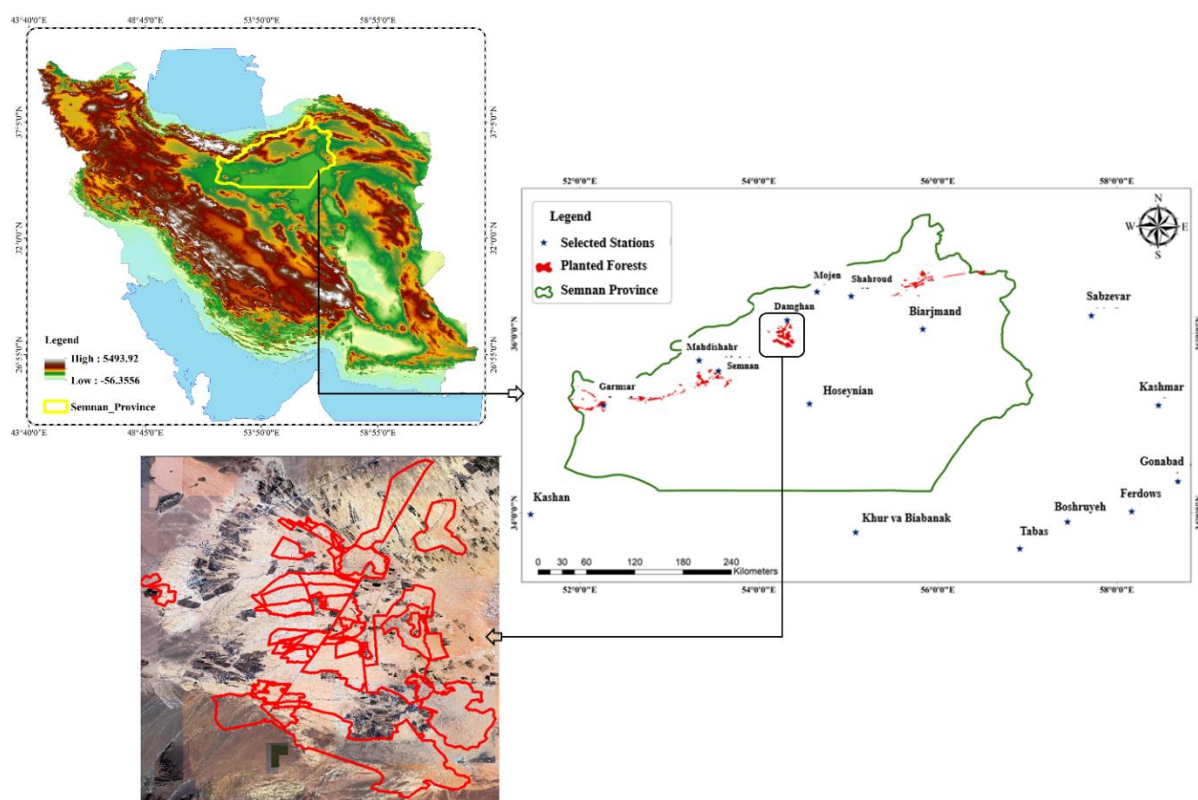
Fig. 1. Geographical location of the study area. (Top Left) Location of Semnan Province within Iran, overlaid on a Digital Elevation Model (DEM) showing topographical variations. (Right) Map of Semnan Province displaying the spatial distribution of the selected synoptic meteorological stations (blue stars) and the extent of Haloxylon spp. afforested zones (red polygons). (Bottom Left) A zoomed-in satellite view of an area.

2.2. Data used
2.2.1. Meteorological data
To evaluate climate variability and compute drought indices, long-term precipitation and temperature records were obtained from selected synoptic stations located within and around Semnan Province, including Semnan, Damghan, Shahrood, and Garmsar, as well as from adjacent provinces. These data were acquired from the Iran Meteorological Organization and span a 30-year statistical period from 1992 to 2022, providing sufficient temporal depth for robust climate analysis. The geographical locations of the stations are shown in Table 1.

Table 1. Synoptic meteorological stations are used for climate analysis in the study area.

Station Name	Latitude	Longitude	Province
Biarjomand	36.05	55.83	Semnan
Semnan	35.58	53.55	
Damghan	36.15	54.32	
Mehdishahr	35.70	53.33	
Majan	36.47	54.65	
Garmsar	35.20	52.27	
Hoseininan	35.22	54.57	
Shahroud	36.42	55.03	
Khour v Biabanak	33.78	55.08	Isfahan
Kashan	33.98	51.45	
Sabzevar	36.20	57.72	Khorasan Razavi
Kashmar	35.20	58.47	
Gonabad	34.35	58.68	
Tabas	33.60	56.92	Khorasan Jonoubi
Boshrouyeh	34.02	58.17	
Ferdos	33.90	57.45	

2.2.2. Satellite data

To assess vegetation canopy conditions and dynamics, Landsat 8 imagery acquired by the Operational Land Imager (OLI) sensor was utilized. These satellite images have spatial resolutions of 15 m (panchromatic) and 30 m (multispectral), with a swath width of approximately 185 km. For this study, 30 m resolution multispectral images were downloaded at 16-day intervals from the United States Geological Survey (USGS) EarthExplorer platform. Remote sensing data were processed to extract four key indices (the Advanced Vegetation Index (AVI), Shade Index (SI), Bare Soil Index (BSI), and Thermal Index (TI)) for the period from 2013 to 2022. These indices provided critical indicators of land degradation trends, allowing for the identification of transitions from afforested zones to shrubland conditions. The study period was defined based on the availability of high-quality satellite imagery and corresponding ground-based meteorological records. While the long-term climatic trends were analyzed over 30 years (1992–2022) to establish baselines, the specific assessment of vegetation dynamics and its response to climate drivers focused on the 2013–2022 timeframe, corresponding to the operational period of the Landsat 8 OLI sensor.

3. Research Methodology

3.1. Preprocessing of satellite images

All Landsat 8 OLI image processing and analysis were implemented within the Google Earth Engine (GEE) cloud computing platform. We used the Surface Reflectance (Collection 2, Level 2) dataset, atmospherically corrected using the Land Surface Reflectance Code (LaSRC) algorithm to ensure consistency across temporal datasets. Additionally, a cloud masking procedure was applied using the Quality Assessment (QA) band to remove cloud and shadow contamination. For spatial harmonization, all images were reprojected to the WGS84 UTM coordinate reference system.

3.2. Calculation of Forest Canopy Density (FCD) Index

To quantitatively evaluate vegetation structure and canopy health, the FCD model was applied using four biophysical indices: AVI, BSI, TI, and SI. These indices collectively reflect vegetation vigor, soil exposure, surface temperature, and canopy shade distribution.

3.3. Advanced Vegetation Index (AVI)

AVI enhances vegetation-structure detection by capturing subtle differences in canopy density. It is computed using the near-infrared (NIR) and red bands. In this study, the index was calculated using the following equation (Rikimaru et al., 2002; Pôças et al., 2013):

$$AVI=[(B_5+1)(256-B_4)(B_5 - B_4)]^{1/3} \tag{1}$$

Where B values represent the top-of-atmosphere (TOA) reflectance (scaled 0–1). This index was computed following the methodology described by Rikimaru et al. (2002). Where B5 and B4 represent the Digital Number (DN) values of the Near-Infrared (NIR) and Red bands of Landsat 8, respectively, the term (256-B4) is used to account for the soil background response, making the index more sensitive to vegetation biomass than traditional indices like NDVI.

3.4. Bare Soil Index (BSI)

BSI is designed to enhance detection accuracy in sparsely vegetated areas where traditional vegetation indices tend to underperform. It is calculated based on spectral reflectance differences between bare soil and vegetation using near-infrared, blue, and red bands (Chen et al., 2004):

$$BSI=((B_4+B_2)-B_3)/((B_4+B_2)+B_3) \tag{2}$$

This index effectively identifies bare surfaces and supports the separation of soil and vegetation signals in dryland ecosystems.

3.5. Thermal Index (TI)

TI provides insight into surface thermal behavior and potential stress on vegetation. Derived from the thermal infrared band, this index measures fluctuations in emitted radiance and surface temperature. The computation follows a multi-step approach using calibration constants specific to the Landsat sensor (Pakkhesal et al., 2013):

$$k_1=666.09 \text{ watts/(m}^2\text{,ster,αm)} \tag{3}$$

$$k_2=1282.71 \text{ (kelvin)} \tag{4}$$

$$L_{min}=0.1238 \text{ watts/(m\textasciicircum2.ster.αm)} \tag{5}$$

$$L_{max}=1.500 \text{ watts/(m}^2\text{.ster.αm)} \tag{6}$$

$$L=L_{min}+[(L_{max}-L_{min})/(255×Q)] \tag{7}$$

In these equations, Q represents the digital number (DN) value from Band 6, L denotes the spectral radiance, k_1 and k_2 are sensor-specific calibration constants, and T refers to the surface temperature in Kelvin.

3.6. Shadow Index (SI)

SI reflects canopy structure by measuring relative shadow intensity across visible bands (Bera et al., 2020). It is instrumental in detecting vegetation arrangement, crown density, and spatial

variation in forest architecture. SI is often used in combination with AVI and BSI for robust forest monitoring and is calculated as:

$$SI=\{(DN_{max}-Blue)(DN_{max}-Green)(DN_{max}-Red)\}^{(1/3)} \tag{8}$$

3.7. Principal Component Analysis (PCA) and Vegetation Density (VD)

To integrate the biophysical indices and quantify the vegetation density, Principal Component Analysis (PCA) was employed. PCA is a multivariate statistical technique widely used in environmental studies in arid regions to reduce data dimensionality and handle correlated variables (Kamali *et al*., 2020). In this study, PCA was applied to the feature space formed by the AVI and BSI. Since vegetation vigor and bare soil exposure typically exhibit a strong negative correlation, the First Principal Component (PC1) captures the majority of the variance and represents the Vegetation Density (VD). Similarly, PCA was performed on the SI and TI layers to derive the Scaled Shadow Index (SSI). The resulting PC scores were standardized to a scale of 0 to 100 using the min-max normalization method.

3.8. Integration of Indices and FCD Calculation

The FCD model provides an efficient approach for generating forest canopy density maps from satellite imagery, expressed as percentage canopy cover. Originally developed by Rikimaru (1996) based on the *Landsat Data Processing Guide for Forest Canopy Density Mapping and Monitoring*, the model has been widely adopted globally since 2002 due to its robustness and simplicity (Sahana *et al*., 2015). It estimates canopy cover directly from Landsat-derived indices, eliminating the need for ground-based training samples for various forest density classes.

Unlike traditional qualitative assessments, the FCD model enables quantitative analysis of forest growth by computing canopy density at the pixel level. The resulting maps offer greater alignment with ground reality and exhibit higher accuracy than those derived from conventional band combinations. This method supports spatially explicit evaluations of forest conditions and provides valuable insight into degradation patterns, recovery potential, and the urgency of restoration interventions (Rikimaru *et al*., 2002).
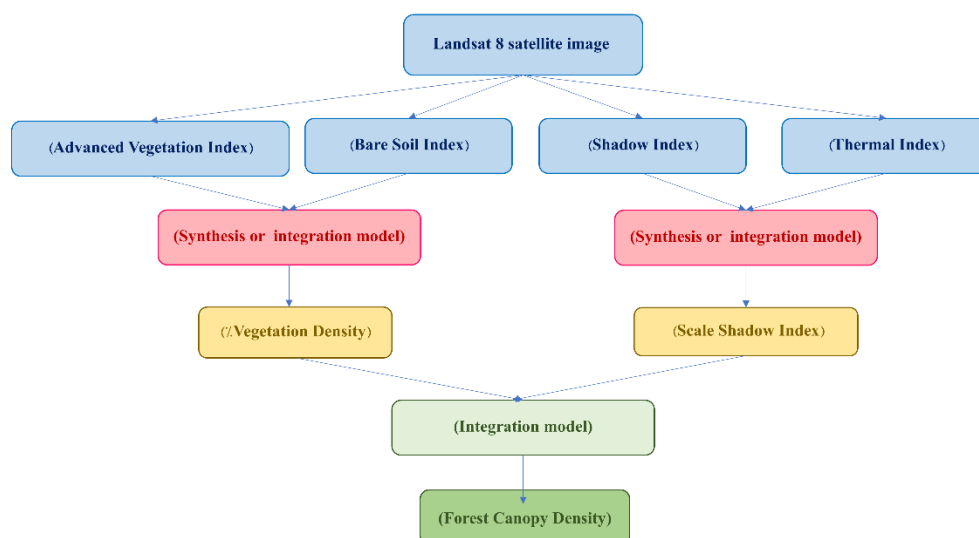
Fig. 2. The processing steps for satellite imagery (Landsat 8 OLI), calculation of Forest Canopy Density

(FCD) indices (AVI, BSI, SI, TI).

FCD values are computed by integrating the SI and VD, both normalized on a 0–100 scale. The combined model yields the final FCD map, with density values expressed as percentages. The FCD calculation is performed using the following equation:

$$FCD = (\sqrt{((VD \times SSI) + 1)}) - 1 \tag{9}$$

In this expression, *VD* refers to the VD index, and *SSI* represents the self-shading index derived from SI. These components were integrated to produce annual FCD maps (0–100%) for each year within the study period, enabling temporal assessment of forest canopy dynamics.

3.9. Analysis of climatic fluctuations using SPEI

To evaluate drought severity and temporal climate variability, the Standardized Precipitation Evapotranspiration Index (SPEI) was computed. SPEI is a multi-scalar drought index based on the climatic water balance (precipitation minus potential evapotranspiration). In this study, Potential Evapotranspiration (PET) was estimated using the Thornthwaite method based on monthly mean temperature and latitude data. The SPEI values were calculated at a 12-month timescale to capture long-term drought patterns, following the standard methodology described by Vicente-Serrano *et al.* (2010). The resulting SPEI time series was computed for each synoptic station and spatially interpolated within a GIS environment to assess drought dynamics across the study area.

The value of *W* is defined as: $W = \sqrt{(-2 \ln P)}$ where $P = 1 - F(x) \leq 0.5$. If $P > 0.5$, it is replaced by 1-P1-P1-P, and the resulting SPEI value is multiplied by -1 to ensure symmetry.

In this study, monthly temperature and precipitation data from 1992 to 2022 were used for all synoptic stations. SPEI values were computed in MATLAB across four temporal scales: 3, 6, 9, and 12 months. The SPEI sign reflects water balance trends, with increasingly negative values indicating more severe drought conditions.

3.10. Correlation analysis

To evaluate the relationship between vegetation dynamics and climatic variability, the Pearson correlation coefficient was computed between FCD and SPEI values for the period 2013–2022. The statistical significance of the correlation coefficients was tested at the 95% confidence level, allowing for the identification of spatial and temporal trends in vegetation response to drought conditions.

The Pearson correlation coefficient R_{xy} is defined as:

$$R_{xy} = \frac{\sum_{i=1}^{n}(x_i - \overline{x})(y_i - \overline{y})}{\sqrt{\sum_{i=1}^{n}(x_i - \overline{x})^2}\sqrt{\sum_{i=1}^{n}(y_i - \overline{y})^2}} \tag{10}$$

In this equation, *x* and *y* represent the paired sample values of the dependent and independent variables (in this case, FCD and SPEI, respectively), $\overline{x}$ *and* $\overline{y}$ denote their means, and *n* is the total number of observations.

While correlation analysis reveals the strength and direction of association between two variables, it does not imply causation. A positive correlation indicates that increases in one variable tend to be associated with increases in the other, whereas a negative correlation implies an inverse relationship. The correlation coefficient ranges from -1 to +1, with values closer to -1 or +1 indicating stronger linear associations.

3.11. Quantification of Climatic and Anthropogenic Impacts

To explicitly quantify and separate the contributions of climate variability and anthropogenic activities to forest canopy changes, the Residual Trend Analysis (RESTREND) method was employed (Evans & Geerken, 2004; Wessels *et al*., 2007). First, a simple linear regression model was established for each pixel to predict the expected Forest Canopy Density (FCD_{pred}) based on the climatic drought index ($SPEI$) as the independent variable:

$$FCDpred = a \times SPEI + b \tag{11}$$

Where a and b These are the regression coefficients. The predicted FCD (FCD_{pred}) represents the vegetation condition expected solely under climatic influence. Next, the residuals (FCD_{res}) were calculated by subtracting the predicted FCD from the observed FCD (FCD_{obs}):

$$FCD_{res} = FCD_{obs} - FCD_{pred} \tag{12}$$

The temporal trends of the calculated residuals (FCD_{res}) were then analyzed to isolate anthropogenic impacts. A statistically significant negative trend in residuals implies vegetation degradation driven by human activities (e.g., overgrazing), whereas a positive trend suggests human-induced improvement (e.g., restoration efforts). A non-significant trend (or trend of zero) indicates that vegetation dynamics are primarily controlled by climatic variability.

4. Results

The results derived from satellite image processing and climate data analysis are presented in this section. First, the spatial distribution of planted forest canopy density was assessed using biophysical indicators. Second, climatic variability was analyzed across the study region. Finally, the relationship between vegetation dynamics and climate fluctuations was examined to understand ecosystem responses.

4.1. Assessment of planted forest density

The indices AVI, BSI, SI, and TI were processed to estimate canopy density. VD was calculated by combining AVI and BSI, while SI and TI were integrated to compute the SSI. Together, VD and SSI were used to estimate FCD values, expressed as pixel-level canopy cover percentages. High AVI values consistently corresponded to higher FCD, whereas low AVI values coupled with high BSI values indicated bare land. Conversely, low BSI values signified vegetated surfaces. SI values were low for shrub-dominated or open areas, highlighting canopy gaps and damage associated with reduced cover. TI increased with decreasing vegetation, reaching higher values in barren landscapes.

VD, defined as the proportion of soil surface shaded by canopy, was derived using principal component analysis (PCA) to address the negative correlation between AVI and BSI. Figure 4 illustrates the mean AVI distribution for the 10-year study period.

4.2. Advanced vegetation index (AVI)

Figure 4 shows the spatial distribution of vegetation health and density across the study area. Patches with high AVI values, representing denser and healthier vegetation, were concentrated within afforested zones and served as relatively stable plantation cores. In contrast, extensive areas exhibited low AVI values, reflecting sparse, stressed, or degraded vegetation.
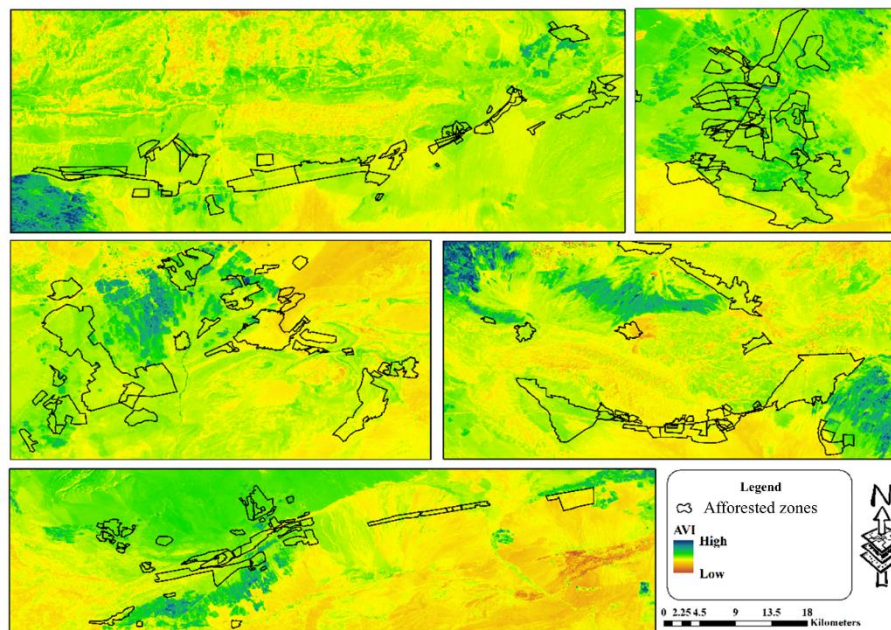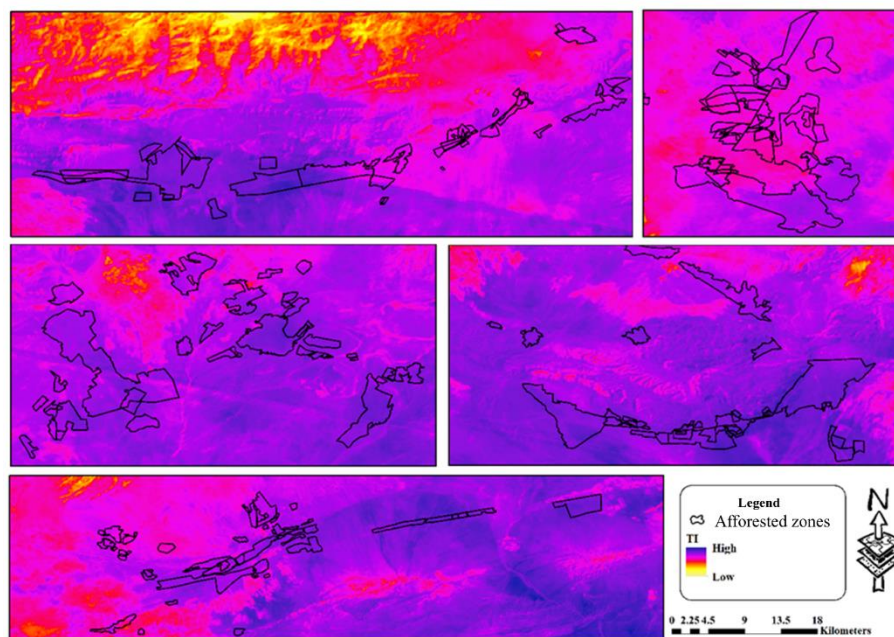
Fig. 3. Spatial distribution of the mean Advanced Vegetation Index (AVI) across the afforested zones of Semnan Province, derived from Landsat 8 OLI imagery (averaged over 2013–2022). High values (blue/green) indicate denser and healthier vegetation clusters, while low values (yellow/orange) correspond to sparse canopies or stressed vegetation areas. The black polygons delineate the boundaries of the planted forests.
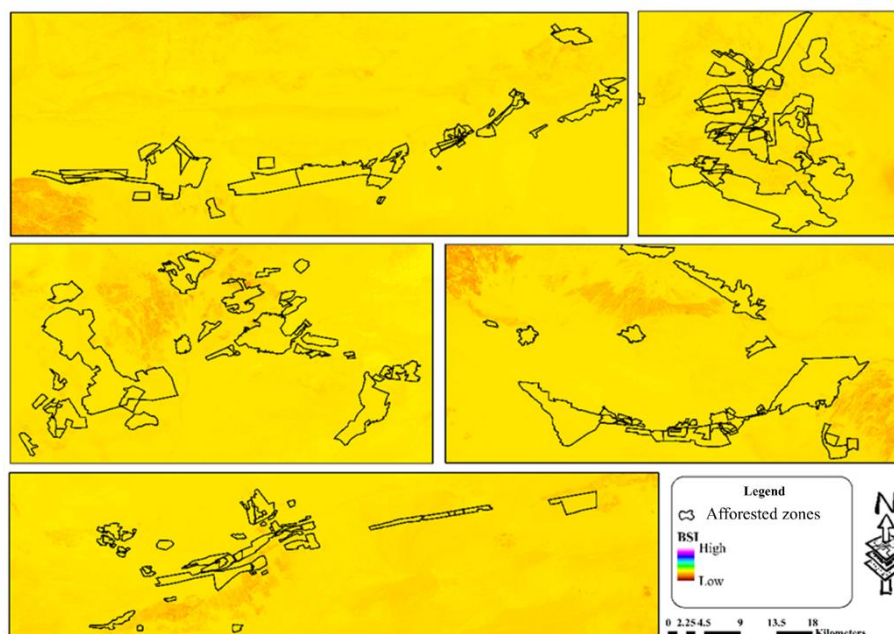
Fig. 4. Spatial distribution of the mean Bare Soil Index (BSI) for the period 2013–2022. High BSI values (blue/purple) represent exposed soil surfaces with minimal vegetation cover, indicating areas highly susceptible to wind erosion. Low values (yellow/orange) correspond to vegetated areas where soil exposure is minimized by canopy cover.

The spatial distribution of vegetation health and canopy density is shown, with high AVI values indicating dense, stable plantation patches. BSI and TI maps (Figures 5 and 6) present inverse vegetation patterns: high BSI values (yellow/orange) coincide with low AVI areas, indicating bare or sparsely vegetated land, while high TI values (blue/purple) correspond to vegetation loss and elevated surface temperatures caused by exposed soil. This negative relationship between vegetation cover and surface temperature is a key indicator of desertification.

High BSI values (yellow to brown) correspond to exposed or sparsely vegetated land, overlapping with areas of low AVI, and indicating extensive bare surfaces within afforested zones.
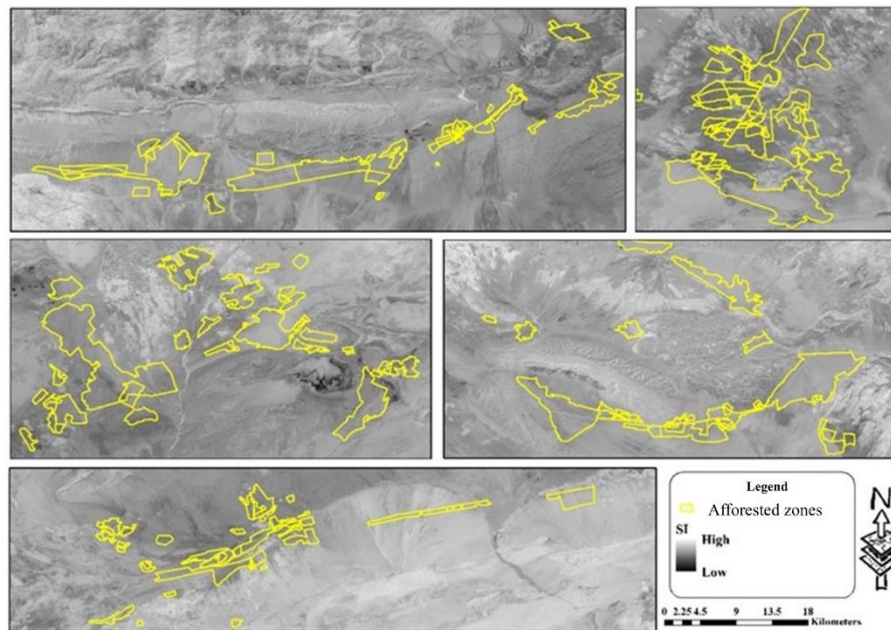

Fig. 5. Spatial distribution of the mean Thermal Index (TI) derived from the thermal infrared band of Landsat 8 (2013–2022). High values (yellow/orange) indicate higher surface temperatures associated with bare soil and sparse vegetation, while low values (purple/blue) correspond to denser vegetation areas with lower thermal emission due to evapotranspiration cooling effects.

Areas with high TI values coincide with zones of low vegetation cover, reflecting elevated surface temperatures due to increased solar absorption by exposed soils. The inverse relationship between TI and vegetation cover highlights thermal signatures of land degradation and desertification.

After generating the TI map, the SI and the advanced SI were produced. The calculation of the advanced SI is the only step in the implementation of the FCD model where the use of simple statistical thresholds, such as the mean, median, or mode, is not recommended. Instead, values are normalized to a 0–100 scale to standardize shadow intensity. In the conventional SI, pixel values may range from 0 to an unrestricted upper limit, whereas in the advanced SI, all values are constrained to 0-100, improving interpretability and comparability. Figure 7 illustrates the SI map, where lighter areas indicate greater canopy shadow and correspondingly higher index values.

Fig. 6. Spatial distribution of the mean Shadow Index (SI) (2013–2022). High SI values (lighter/white tones) indicate areas with greater canopy shadow intensity, reflecting a more complex and multi-layered forest structure. Low values (darker/black tones) represent open or flat terrain with minimal vertical vegetation structure.
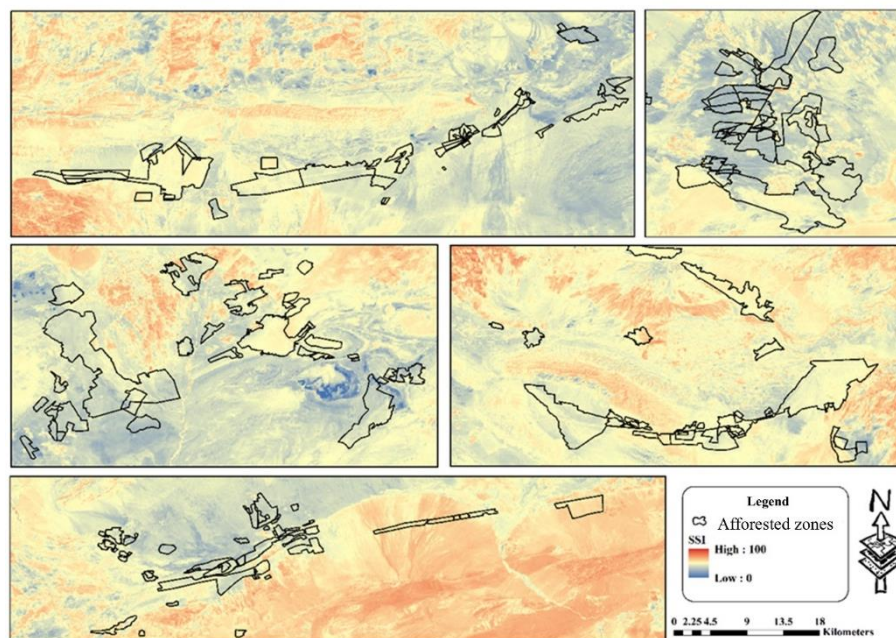
Fig. 7. Spatial distribution of the Scaled Shadow Index (SSI), obtained by integrating the Shadow Index (SI) and Thermal Index (TI) using Principal Component Analysis (PCA). This index enhances the differentiation of vegetation canopy from other dark surface features. High SSI values indicate areas with dense forest canopy, characterized by high shadow intensity and relatively lower surface temperatures, whereas low SSI values correspond to open areas with minimal vegetation shading.

Lighter areas indicate higher SI values, reflecting greater canopy shading and denser vegetation. PCA integration was then applied to the combined SI and TI layers to derive the SSI map (Figure 8). This integration enhances canopy detection by capturing both shading and surface temperature effects.

Similarly, AVI and BSI were integrated using PCA to generate VD. Given the negative correlation between AVI and BSI, the first principal component (PC1) was selected as the basis for VD. The transformation standardized vegetation density across the landscape, assigning values near 0 to bare-land pixels and values near 100 to areas with the densest vegetation.
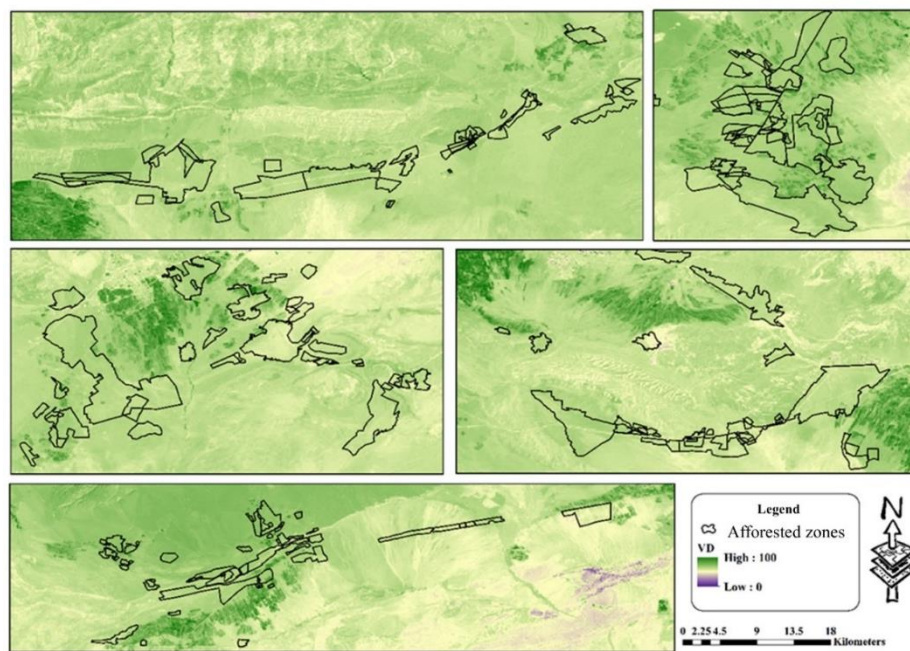

Fig. 8. Spatial distribution of Vegetation Density (VD) derived from the Principal Component Analysis (PCA) of AVI and BSI indices. High VD values correspond to areas with dense vegetation cover and minimal soil exposure, while low VD values indicate sparse vegetation or bare soil.

The final FCD map (Figure 9) quantified the vegetation structure of the planted forests. The analysis revealed that the canopy density within the afforested zones ranged from 44.97% to 55.78%. This indicates that the Haloxylon spp. plantations have maintained a moderate and relatively uniform canopy structure across the study area. Unlike natural forests, which may exhibit extreme density variations, these man-made stands show a consistent cover typical of established desert plantations, with no areas falling into the sparse (<10%) or closed (>60%) density classes.

4.3. SPEI results

The temporal analysis of the Standardized Precipitation-Evapotranspiration Index (SPEI) revealed significant fluctuations in moisture availability over the study period (2013–2022). As illustrated in Figure 10, the region experienced severe and prolonged drought conditions, particularly towards the end of the decade. The most severe drought year was 2022, where the SPEI reached its lowest values across all time scales, with an annual average of -2.28 for SPEI-9 and -2.22 for SPEI-12, indicating extreme hydrological stress. Conversely, a brief wet period was observed in 2019 and 2020, with SPEI values peaking at approximately +1.46 (SPEI-3).
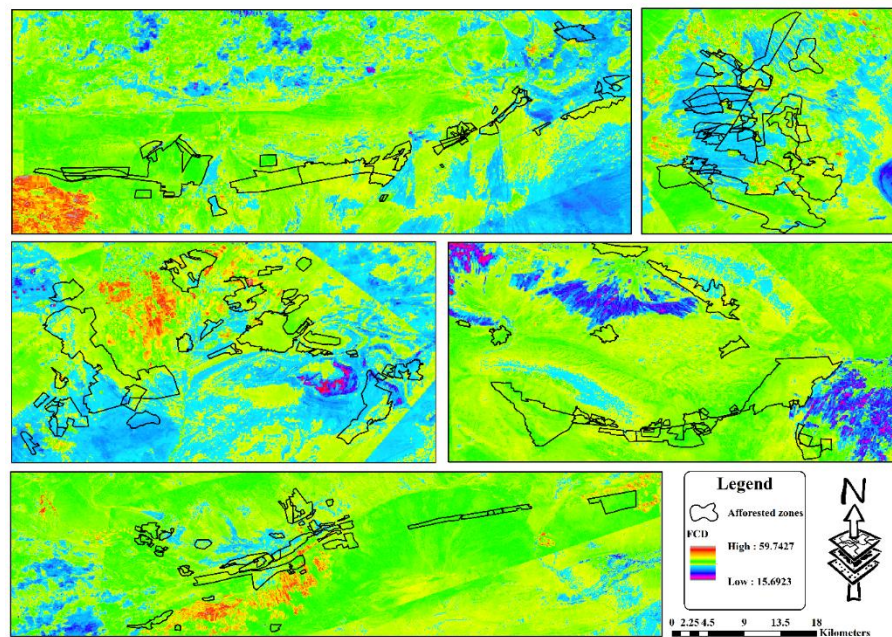
Fig. 9. Final Forest Canopy Density (FCD) map of the planted forests in Semnan Province, averaged over the 2013–2022 period. The map classifies canopy density into percentages. High values represent high-density forest patches (>60%), while low values (yellow/orange) indicate low-density or degraded stands (<30%). This map serves as the primary indicator of vegetation status for further analysis
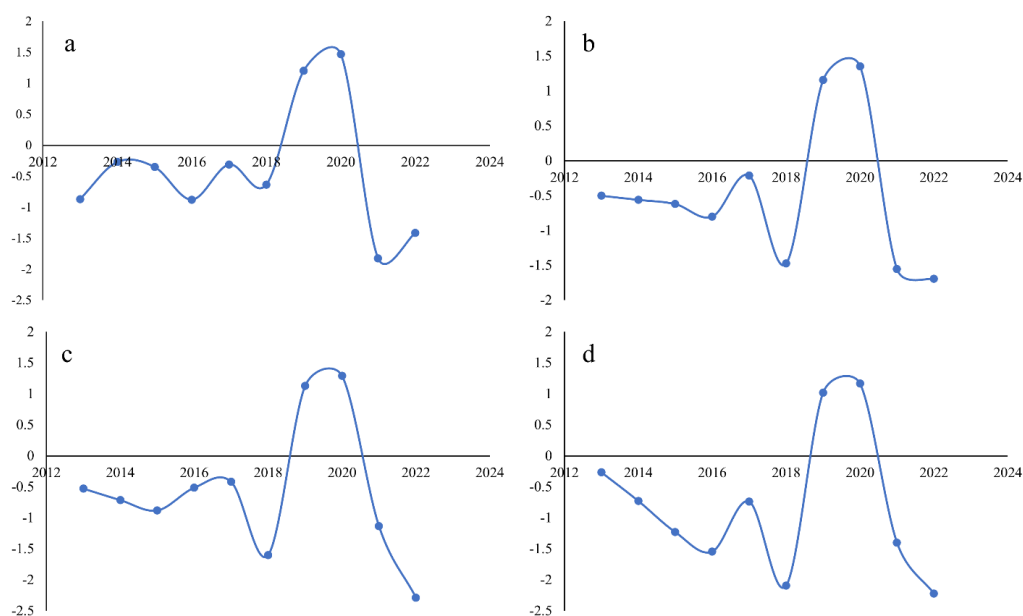
Fig. 10. Temporal variation of the Standardized Precipitation-Evapotranspiration Index (SPEI) at different time scales: (a) 3-month, (b) 6-month, (c) 9-month, and (d) 12-month, for the period 2013–2022. Positive values (above zero) indicate wet periods, while negative values (below zero) denote drought conditions. The prolonged drought event from 2013 to 2018 is evident across all time scales.

4.4. Relationship between climate and forest health: correlation analysis

The correlation analysis (Table 2) indicated that forest canopy density was not significantly influenced by precipitation variability over the 10 years. Although the highest correlation coefficient was observed at the 9-month lag (R = 0.21), it was not statistically significant (p = 0.56, n = 10). This weak coupling suggests that vegetation in the study area is largely decoupled from short-term atmospheric precipitation.

Table 2. Pearson correlation coefficients (R) between FCD and SPEI at various time scales.

Timescale	SPEI-3	SPEI-6	SPEI-9	SPEI-12
Correlation (R)	0.03	0.08	0.21*	0.17
p-value	0.935	0.826	0.561	0.638
Sample Size (n)	10	10	10	10

Lagged Climate Response. The strongest significant correlation was observed at a 9-month timescale (R = 0.21). This indicates that the response of desert plantations to precipitation variability is delayed rather than immediate. In particular, *Haloxylon* spp. requires extended periods of soil moisture accumulation, typically during autumn and winter, to manifest positive growth responses in the subsequent spring and summer. Thus, the 9-month lag most accurately captures the cumulative effect of precipitation on vegetation dynamics.

Spatial Heterogeneity. The spatial correlation map (Figure 11) shows that the relationship between climate and forest health is not uniform across space. Strong positive correlations are concentrated in the central and eastern plantation zones, where climate exerts dominant control and human disturbances appear limited. Conversely, weak or negative correlations emerge in other areas, suggesting that non-climatic pressures (such as groundwater depletion, overgrazing, and poor management) have offset the benefits of favorable rainfall, resulting in continued canopy decline.

### 4.5. Attribution of vegetation changes to climate and human factors

To isolate the role of anthropogenic drivers, the residuals (difference between observed and climate-predicted FCD) were analyzed for temporal trends using the Mann-Kendall test (Figure 12). The resulting Z-statistics ranged from -1.40 to +1.40 across the study area. Since these values fall within the range of non-significant trends (-1.96 < Z < +1.96 at 95% confidence level), no statistically significant anthropogenic degradation or improvement trends were detected. This suggests that while human activities (degradation or restoration) are present, they have not caused a statistically abrupt shift in the ecosystem state during this specific 10-year period, implying a relative stability in human pressures.

5. Discussion

This study assessed the sustainability of desert plantations in Semnan Province and disentangled the relative contributions of climate variability and human activities. The discussion is organized to address the three key research questions posed in the introduction.
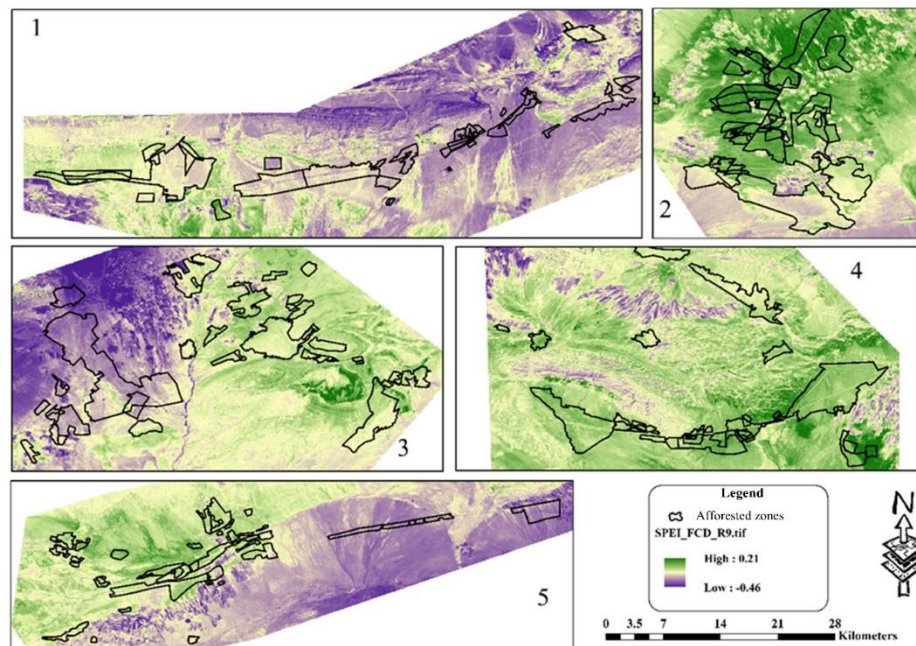
Fig. 1. Spatial distribution of the Pearson correlation coefficients (R) between Forest Canopy Density (FCD) and the 9-month Standardized Precipitation-Evapotranspiration Index (SPEI-9) across the study area (2013–2022). Green pixels indicate positive correlations where vegetation dynamics follow climatic trends, while purple pixels show weak or negative correlations, suggesting the decoupling of vegetation from climate due to non-climatic factors (e.g., groundwater or human impact).
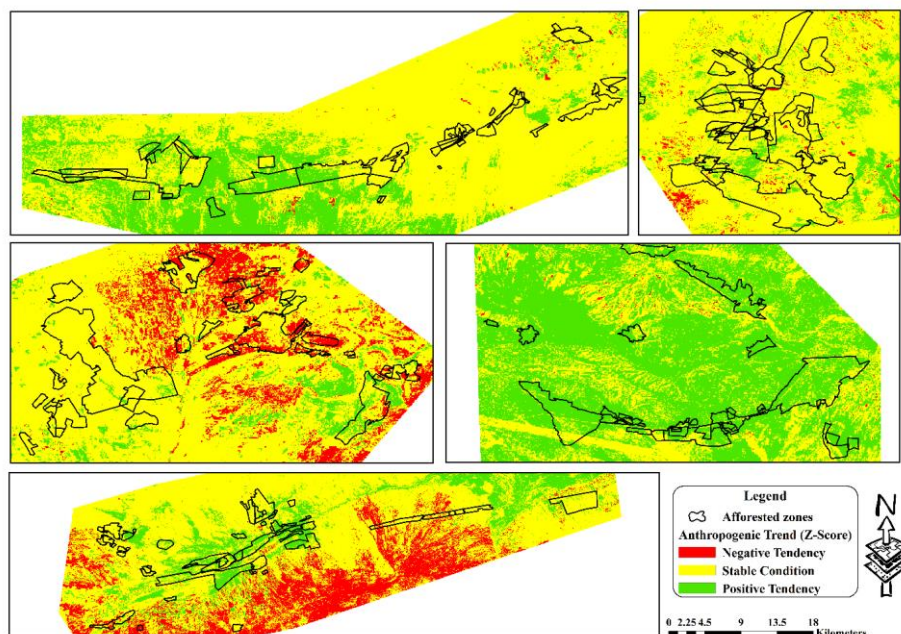
Fig. 12. Spatial distribution of the trends in anthropogenic impacts on forest canopy density (2013–2022), derived from the Residual Trend Analysis (RESTREND). This map illustrates the Mann-Kendall Z-statistics calculated for the time series of residuals (the difference between observed FCD and climate-predicted FCD).

5.1. Spatial and Temporal Trends in Forest Canopy

A key outcome is the heterogeneous spatial distribution of FCD. Although afforestation is widely recognized as an effective strategy for combating desertification (Chen *et al*., 2019), our results show that its success is highly contingent upon local ecological conditions. The observed FCD range (45–56%) suggests that despite the harsh environmental conditions, the plantations have successfully established a moderate canopy cover, avoiding severe degradation (low density < 10%) or collapse. This consistency in canopy density contrasts with some reports from other arid regions where large-scale plantations faced massive dieback (Chai *et al*., 2019), indicating a relatively high resilience of the planted species in Semnan Province.

5.2. Attribution of Changes: Climate vs. Human Drivers

Regarding the role of climate, our analysis showed no statistically significant correlation between SPEI and FCD (R = 0.21, p > 0.05, N = 10). While an R-value of 0.21 suggests a slight positive tendency at a 9-month lag, the lack of statistical significance indicates that precipitation variability is not the primary driver of vegetation dynamics in this system. This finding supports the hypothesis of ecological decoupling, where deep-rooted species, such as Haloxylon spp. rely more on groundwater stability than on transient rainfall events. Consequently, the observed canopy dynamics are likely governed by non-climatic factors (Alamdarloo *et al*., 2018; Jiang *et al*., 2022).

5.3. Hotspots of Degradation and Resilience

The spatial analysis utilizing RESTREND provided further insight into the anthropogenic footprint. Contrary to expectations of rapid degradation, the Mann-Kendall trend test on residuals revealed no statistically significant trends (Z-values ranging from -1.40 to +1.40) across the entire study area. This absence of significant trends indicates a state of relative stability, suggesting that anthropogenic pressures—such as grazing intensity and groundwater extraction—have remained constant rather than intensifying during the 2013–2022 period.

This observation aligns with findings from Kundu *et al*. (2017) in India and Zhang *et al*. (2016) in Inner Mongolia, where anthropogenic drivers were identified as major determinants of desertification processes. In the present study area, although no distinct "degradation hotspots" (characterized by significant negative trends) were statistically identified, the overall low canopy density suggests that the ecosystem is maintained in a fragile state due to chronic human pressures, preventing significant recovery even during favorable climatic episodes (Behrangmanesh *et al*., 2019).

It is important to acknowledge certain limitations of this study. First, while the FCD model provides a robust proxy for canopy density, the lack of extensive historical ground-truth data limited our ability to perform a pixel-by-pixel validation for older dates. Second, although the Residual Trend Analysis (RESTREND) allowed us to isolate human impacts, we did not directly quantify specific human activities (e.g., pumping rates or grazing intensity) due to data scarcity. Future research should integrate socio-economic data and groundwater modeling to further refine the attribution of these anthropogenic drivers.

6. Conclusion

This study evaluated the sustainability of planted aridland forests in Semnan Province by distinguishing the relative roles of climate variability and human activities. The findings reveal that these forests have maintained a moderate canopy density despite environmental stressors.

The analysis demonstrated a non-significant correlation between canopy density and climatic drought indices ($P > 0.05$), highlighting the decoupling of vegetation from precipitation and the dominance of anthropogenic stressors. Furthermore, the Residual Trend Analysis indicated no significant trend in human impacts, suggesting a status quo of chronic pressure rather than rapid recent degradation.

Therefore, to ensure long-term sustainability, management strategies must move beyond general conservation goals to specific, actionable measures. Prioritized interventions should include: (1) enforcing strict groundwater quotas and shutting down illegal wells within a 5-km buffer of afforested zones to restore the water table; (2) implementing rotational grazing schemes that strictly exclude livestock during critical regeneration periods (spring and early summer); and (3) adopting drought-adaptive silvicultural practices, such as thinning of senescent stands to reduce water competition. Without these targeted interventions, adaptation to climate variability alone will be insufficient to secure the persistence of these critical national assets.

Author Contributions
Mohsen Abdolhoseini and: Writing – original draft, Methodology, Investigation, Formal analysis, Data curation, Conceptualization. Hassan Khosravi and Ali Tavili: Conceptualization, Investigation, Methodology, Project administration, Supervision, Writing – review & editing. Gholamreza Zehtabian and Hamidreza Keshtkar: Conceptualization, Investigation, Methodology and Esmaeil Heydari Alamdarlou: Methodology, Investigation, Formal analysis, Data curation, Conceptualization.

Data Availability Statement
Do not have any research data outside the submitted manuscript file.

Ethical considerations
Not applicable.

Conflict of interest
The authors declare that they have no conflicts of interest.

References

Alamdarloo, E. H., Manesh, M. B., & Khosravi, H. (2018). Probability assessment of vegetation vulnerability to drought based on remote sensing data. *Environmental Monitoring and Assessment, 190(12),* 702. https://doi.org/10.1007/s10661-018-7089-1

Ataei, H., & Hasheminasab, S. (2012). The Regionalization and the Evaluation of human bioclimatic of Semnan Province. *Journal of Urban Ecology Research*, 3(6), 19-36.

Azizi, Z., Najafi, A., & Sohrabi, H. (2008). Forest canopy density estimation, using satellite images. The International Archives of the Photogrammetry. *Remote Sensing and Spatial Information Sciences, 37*, 1127-1130

Barati, A. A., Pour, M. D., & Sardooei, M. A. (2023). Water crisis in Iran: A system dynamics approach on water, energy, food, land and climate (WEFLC) nexus. *Science of the Total Environment, 882*, 163549. https://doi.org/10.1016/j.scitotenv.2023.163549

Behrang Manesh, M., Khosravi, H., Azarnivand, H., & Senatore, A. (2019). Quantifying the trend of vegetation changes using remote sensing (Case study: Fars Province). *Journal of Plant Ecosystem Conservation, 7(15)*, 295-318. http://pec.gonbad.ac.ir/article-1-565-en.html

Bera, B., Saha, S., & Bhattacharjee, S. (2020). Estimation of forest canopy cover and forest fragmentation mapping using Landsat satellite data of Silabati River Basin (India). *Journal of Cartography and Geographic Information, 70 (4)*, 181-197. https://doi.org/10.1007/s42489-020-00060-1

Chai, Q., Ma, Z., An, Q., Wu, G. L., Chang, X., Zheng, J., & Wang, G. (2019). Does Caragana korshinskii plantation increase soil carbon continuously in a water-limited landscape on the Loess Plateau, China?. *Land Degradation & Development, 30(14),* 1691-1698. https://doi.org/10.1002/ldr.3373

Chen, C., Park, T., Wang, X., Piao, S., Xu, B., Chaturvedi, R. K., ... & Myneni, R. B. (2019). China and India lead in greening of the world through land-use management. *Nature Sustainability, 2(2)*, 122-129. https://doi.org/10.1038/s41893-019-0220-7

Chen, J., Jönsson, P., Tamura, M., Gu, Z., Matsushita, B., & Eklundh, L. (2004). A simple method for reconstructing a high-quality NDVI time-series data set based on the Savitzky-Golay filter. *Remote sensing of Environment, 91(3-4),* 332-344. https://doi.org/10.1016/j.rse.2004.03.014

Chen, W., Yu, T., Han, T., Zhao, C., Li, H., Liu, X., ... & Zhang, X. (2023). Effects of afforestation by aerial sowing on topsoil physicochemical properties in the sandy desert, NW China. *Journal of Soils and Sediments, 23(6),* 2417-2427. https://doi.org/10.1007/s11368-023-03486-y

Eskandari Damaneh, H., Gholami, H., Mahdavi, R., Khoorani, A., & Li, J. (2022). Evaluation of land degradation trend using satellite imagery and climatic data (Case study: Fars province). *Desert Ecosystem Engineering, 8(24),* 49-64. https://deej.kashanu.ac.ir/article_112688.html#:~:text=10.22052/DEEJ.2018.7.24.35

Eskandari, H., Borji, M. Khosravi, H. & Mesbahzadeh, T. (2016). Desertification of forest, range and desert in Tehran province, affected by climate change. *Solid Earth. 7*, 905–915. https://doi.org/10.5194/se-7-905-2016

Evans, J., & Geerken, R. (2004). Discrimination between climate and human-induced dryland degradation. *Journal of arid environments, 57(4),* 535-554.

Ghazvinian, H., Bahrami, H., Ghazvinian, H., & Heddam, S. (2020). Simulation of Monthly Precipitation in Semnan City Using ANN Artificial Intelligence Model. *Journal of Soft Computing in Civil Engineering, 4(4),* 36-46.

Guo, Z., Huang, N., Dong, Z., Van Pelt, R. S., & Zobeck, T. M. (2014). Wind erosion induced soil degradation in Northern China: Status, measures and perspective. *Sustainability, 6(12),* 8951-8966. https://doi.org/10.3390/su6128951

Jain, S., Srivastava, A., Khadke, L., Chatterjee, U., & Elbeltagi, A. (2024). Global-scale water security and desertification management amidst climate change. *Environmental Science and Pollution Research, 31(49),* 58720-58744. https://doi.org/10.1007/s11356-024-34916-0

Jiang, H., Xu, X., Zhang, T., Xia, H., Huang, Y., & Qiao, S. (2022). The relative roles of climate variation and human activities in vegetation dynamics in coastal China from 2000 to 2019. *Remote Sensing, 14(10),* 2485. https://doi.org/10.3390/rs14102485

Jiang, L., Bao, A., Guo, H., & Ndayisaba, F. (2017). Vegetation dynamics and responses to climate change and human activities in Central Asia. *Science of the Total Environment, 599,* 967-980. https://doi.org/10.1016/j.scitotenv.2017.05.012

Jiang, Y., & Arnold, H. (2023). Traditional Water Systems Informing Sustainable Contemporary Drylands Design: Documentation, *Extraction, and Deployment. Sustainability, 15(14),* 10966. https://doi.org/10.3390/su151410966

Kamali, K., Zehtabian, G., Mesbahzadeh, T., Arkhazloo, H. S., Arabkhedri, M., & Moghaddamnia, A. (2020). Assessment of Soil Sustainability Indices in Desert Areas (Case Study: Rangeland and Agricultural Lands of Semnan County). *Journal of Range and Watershed Management, 73(1),* 183-198

Kompas, T., Che, T. N., & Grafton, R. Q. (2024). Global impacts of heat and water stress on food production and severe food insecurity. *Scientific Reports, 14(1),* 14398. https://doi.org/10.1038/s41598-024-65274-z

Kundu, N. R., Patel, S. K., Saha, D. (2017). Desertification in western Rajasthan (India): an assessment using remote sensing-derived rain-use efficiency and residual trend methods. *Natural Hazards. 86(1),* 297-313. https://doi.org/10.1007/s11069-016-2689-y

Li, C., Fu, B., Wang, S., Stringer, L. C., Zhou, W., Lu, T., ... & Ren, Z. (2024). Structure and Functioning of China's Dryland Ecosystems in a Changing Environment. *Dryland Social-Ecological Systems in Changing Environments*, *19;47*, 215–237. https://doi: 10.1146/annurev-ecolsys-121415-032311

Mirzaeizadeh, V., Niknezhad, M., & Hojati, S M. (2015). Estimation of forest canopy density using FCD, *Ecology of Iran Forests. 3(5)*, 63-75. http://ifej.sanru.ac.ir/article-1-188-fa.html

Pakkhesal, E., & Bonyad, A. E. (2013). Classification and delineating natural forest canopy density using FCD model (Case study: Shafarud area of Guilan). *Iranian Journal of Forest and Poplar Research, 21(1)*, 99-114. https://doi.org/10.22092/ijfpr.2013.3815

Pôças, I., Cunha, M., Pereira, L. S., & Allen, R. G. (2013). Using remote sensing energy balance and evapotranspiration to characterize montane landscape vegetation with focus on grass and pasture lands. *International Journal of Applied Earth Observation and Geoinformation, 21*, 159-172. https://doi.org/10.1016/j.jag.2012.08.017

Ravanbakhsh, H., Jafari, A., & Monazami, M. (2023). Irano-Turanian afforestation in Semnan Province, Iran. *Nature of Iran, 8(2)*, 33-38.

Rikimaru, A. (1996) LANDSAT TM Data Processing Guide for Forest Canopy Density Mapping and Monitoring Model. ITTO Workshop on Utilization of Remote Sensing in Site Assessment and Planning for Rehabilitation of Logged-Over Forests, Bangkok, 30 July-1 August 1996, 1-8.

Rikimaru, A., Roy, P.S., & Miyatake, S. (2002). Tropical forest cover density mapping. *Tropical Ecology, 43(1)*, 39-47.

Rosińska, W., Jurasz, J., Przestrzelska, K., Wartalska, K., & Kaźmierczak, B. (2024). Climate change's ripple effect on water supply systems and the water-energy nexus–A review. *Water Resources and Industry, 32*, 100266. https://doi.org/10.1016/j.wri.2024.100266

Sahana, M., Sajjad, H., & Ahmed, R. (2015). Assessing spatio-temporal health of forest cover using forest canopy density model and forest fragmentation approach in Sundarban reserve forest, India. *Modeling Earth Systems and Environment, 1(4),* 1-10. https://doi.org/10.1007/s40808-015-0043-0

Stavi, I., Priori, S., & Thevs, N. (2022). Impacts of climate change and land-use on soil functions and ecosystem services in drylands. *Frontiers in Environmental Science, 10*, 851751. https://doi.org/10.3389/fenvs.2022.851751

Su, Y. Z., Zhao, W. Z., Su, P. X., Zhang, Z. H., Wang, T., & Ram, R. (2007). Ecological effects of desertification control and desertified land reclamation in an oasis-desert ecotone in an arid region: a case study in Hexi Corridor, northwest China. *Ecological Engineering, 29(2),* 117-124. https://doi.org/10.1016/j.ecoleng.2005.10.015

United Nations Convention to Combat Desertification (UNCCD). (1994). United Nations Convention to Combat Desertification in those countries experiencing serious drought and/or desertification, particularly in Africa.

Vicente-Serrano, S. M., Beguería, S., & López-Moreno, J. I. (2010). A multiscalar drought index sensitive to global warming: the standardized precipitation evapotranspiration index. *Journal of climate, 23(7),* 1718-1696. https://doi.org/10.1175/2009JCLI2909.1

Wessels, K. J., Prince, S., Malherbe, J., & Small, J. (2007). Trends in land degradation in South Africa 1981–2000. *Remote Sensing of Environment, 110(2)*, 220-235. https://doi.org/10.1016/j.jaridenv.2006.05.015

Wu, B., Smith, W. K., & Zeng, H. (2024). Dryland Dynamics and Driving Forces. In Dryland Social-Ecological Systems in Changing Environments (pp. 23-68). Singapore: Springer Nature Singapore.35. Li, C., Fu, B., Wang, S., Stringer, L. C., Zhou, W., Lu, T., Wu, X., Hu, R., & Ren, Z. (2024). Structure and Functioning of China's Dryland Ecosystems in a Changing Environment. In B. Fu & M. Stafford-Smith (Eds.), Dryland Social-Ecological Systems in Changing Environments (pp. 391–424). Springer. https://doi.org/10.1007/978-981-99-9375-8_12

Ye, Z., Yin, S., Cao, Y., & Wang, Y. (2024). AI-driven optimization of agricultural water management for enhanced sustainability. *Scientific Reports, 14*, 25721. https://doi.org/10.1038/s41598-024-76915-8

Yin, W., Hu, Q., Liu, J., He, P., Zhu, D., & Boali, A. (2024). Assessing Climate and Land-Use Change Scenarios on Future Desertification in Northeast Iran: A Data Mining and Google Earth Engine-Based Approach. *Land, 13(11),* 1802. https://doi.org/10.3390/land13111802

Zeng, H., Wu, B., Elnashar, A., & Fu, Z. (2024). Dryland Dynamics in the Mediterranean Region. In B. Fu & M. Stafford-Smith (Eds.), Dryland Social-Ecological Systems in Changing Environments (pp. 243–271). Springer. https://doi.org/10.1007/978-981-99-9375-8_8

Zhang, M., Liu, S., Jones, J., Sun, G., Wei, X., & Ellison, D.(2022). Managing the forest-water nexus for climate change adaptation. *Forest Ecology and Management, 525*, 120545. https://doi.org/10.1016/j.foreco.2022.120545

Zhang, Y., Huang, K., Zhang, J., Zhao, R., Ojima, D. S., Gao, J., & Zhu, Y. (2024). Dryland Social-Ecological Systems in Americas. In B. Fu & M. Stafford-Smith (Eds.), Dryland Social-Ecological Systems in Changing Environments (pp. 325–357). Springer. https://doi.org/10.1007/978-981-99-9375-8_10

Zhang, Y., Zhang, C., Wang, Z., Chen, Y., Gang, C., An, R., & Li, J. (2016). Vegetation dynamics and its driving forces from climate change and human activities in the Three-River Source Region, China, from 1982 to 2012. *Science of the Total Environment, 563*, 210-220. https://doi.org/10.1016/j.scitotenv.2016.03.223

Ziadat, F., Conchedda, G., Haddad, F., Njeru, J., Brès, A., Dawelbait, M., & Li, L. (2025). Desertification and Agrifood Systems: Restoration of Degraded Agricultural Lands in the Arab Region. *Agriculture*, *15(12),* 1249. https://doi.org/10.3390/agriculture15121249